Research Square

Preprints are preliminary reports that have not undergone peer review.
They should not be considered conclusive, used to inform clinical practice,
or referenced by the media as validated information.

Analysis of Torsional Waves in Multilayered Media with Fibre-Reinforced Magnetoelastic and Pre-Stressed Poroelastic Layers with Sliding Interface over Heterogeneous Elastic Half-Space

Dinesh Kumar Majhi
Patna College, Patna University
Anurag Rakesh
anuragrakesh361@gmail.com

Patna University
Mostaid Ahmed
VIT Bhopal University
Sunny Kumar
Patna University

Research Article

Keywords: Torsional surface waves, fibre-reinforcement, magnetoelasticity, poroelasticity, exponential heterogeneity, sliding interface

Posted Date: May 11th, 2026

DOI: https://doi.org/10.21203/rs.3.rs-9094159/v1

License: This work is licensed under a Creative Commons Attribution 4.0 International License.
Read Full License

Additional Declarations: No competing interests reported.

Analysis of Torsional Waves in Multilayered Media with Fibre-Reinforced Magnetoelastic and Pre-Stressed Poroelastic Layers with Sliding Interface over Heterogeneous Elastic Half-Space

Dinesh Kumar Majhi[1], Anurag Rakesh[2, *], Mostaid Ahmed[3], Sunny Kumar[4]

[1]Department of Mathematics, Patna College, Patna University, Patna - 800005, India.

[2, 4]Department of Mathematics, Patna University, Patna - 800005, India.

[3]School of Advanced Sciences & Languages, VIT Bhopal University, Kothrikalan, Sehore, Madhya Pradesh - 466114, India.

[*]Email: anuragrakesh361@gmail.com

ABSTRACT:

This paper investigates torsional wave propagation in multilayered structure having a fibre-reinforced magnetoelastic layer, an initially stressed anisotropic poroelastic layer, and an exponentially varying heterogeneous elastic half-space. A sliding interface is incorporated between the upper and intermediate layers to model varying interfacial bonding conditions. The governing equations are formulated using fibre-reinforced, magnetoelastic and Biot's poroelastic theories, and a dispersion relation is derived under appropriate boundary conditions. The dispersion relation obtained describes relation of normalized phase velocity on dimensionless wavenumber and key physical parameters, including dimensionless magnetoelastic coupling, reinforcement orientation, porosity, non-dimensional initial stress, interfacial sliding, and dimensionless heterogeneity. The formulation is validated by reducing it to the classical Love wave equation under limiting cases.

Numerical analysis reveals that magnetoelastic coupling, fibre alignment along the propagation direction, interfacial sliding, and rigidity heterogeneity increase phase velocity, whereas porosity, initial stress, density heterogeneity, and layer thickness decrease it. The results consistently exhibit dispersive behavior, with phase velocity decreasing as wavenumber increases. The study provides insights into wave propagation in complex layered media, with applications in geophysics and material characterization.

KEYWORDS: Torsional surface waves, fibre-reinforcement, magnetoelasticity, poroelasticity, exponential heterogeneity, sliding interface

1. INTRODUCTION

Analysis of surface waves has been a central topic in seismology, geophysics, and applied mechanics for over a century. Love's pioneering work on these waves laid the foundation of subsequent theoretical and practical advancements in wave mechanics [1]. Later, Biot [2] introduced influence of pre-stresses on wave propagation, while Weiskopf [3] and Biot [4], [5] extended the framework to porous and fluid-saturated media, thereby providing a comprehensive basis for analysing complex geological formations.

Ewing et al. [6], Biot [7], and Bath [8] further developed wave propagation in stratified structures, whose works have played a vital role in geophysical exploration and earthquake engineering. In parallel, the influence of magnetoelasticity on wave motion was studied extensively, with contributions by Chakrabarti [9] and Chandrasekharaiah [10], highlighting the role of electromagnetic fields on torsional wave characteristics. Achenbach [11] further advanced the understanding of wave propagation in elastic solids, particularly in anisotropic media. Belfield et al. [12] investigated stress distributions in elastic plates with fibre-reinforcement in concentric circles, highlighting its influence on the overall elastic behaviour of the medium.

Over the past few decades, a significant body of literature has emerged on torsional surface waves in various complex media. Gupta and co-workers have investigated torsional wave propagation under influences of initial stress, poroelasticity, boundary irregularities [13] - [17], while Kakar and Kakar [18] explored the combined role of fibre reinforcement and magnetic fields. More recent studies have addressed wave motion in non-homogeneous and viscoelastic structures [19] - [21], as well as the role of boundary configurations such as corrugated interfaces [22] and sliding contact conditions [23], [24]. The work of Pramanik and Manna [25] presents a comprehensive investigation in a complex medium incorporating initial stress, aeolotropy (anisotropy), heterogeneity, irregularity, and porosity. Majhi et al. [26], [27] analysed the combined influence of non-homogeneity and initial stress in a multilayered poroelastic system bounded by heterogeneous structures, showing the complexity introduced by coupled mechanical parameters, for torsional and Love waves.

Despite these contributions, relatively limited attention has been given to the combined effects of fibre-reinforcement, magnetoelasticity, poroelasticity, and exponential heterogeneity within a multilayered system. Moreover, the presence of a sliding interface between layers, which models partial bonding in real-world geological formations and engineering structures, adds further complexity to the wave dynamics. Understanding such systems is crucial for applications in earthquake engineering, seismic exploration, and non-destructive material evaluation.

The present work investigates torsional wave propagation in multilayered media comprising a fibre-reinforced magnetoelastic (FRME) layer, an anisotropic poroelastic layer with initial stress,

and an exponentially heterogeneous half-space. A sliding interface, characterized by a dimensionless parameter, is incorporated to model different interfacial bonding conditions ranging from welded to smooth contact. The derived dispersion relation is analysed under general conditions, and various particular cases are discussed to demonstrate the reduction to existing classical results which further validates the model. Numerical computations illustrate the influence of reinforcement, magnetoelasticity, porosity, heterogeneity, and sliding on torsional wave velocity.

2. FORMULATION

This study looks into transmisssion of torsional waves in multilayered media comprising two distinct layers and a half-space with complex material characteristics. The upper layer M_1 is a finite (depth H_2) fibre-reinforced magnetoelastic (FRME) medium, capturing the coupled effects of elasticity, reinforcement, and magnetic fields. Beneath it lies a finite (depth H_1), fluid-saturated, anisotropic porous layer M_2 of Weiskopf type, having initial compressive stress P. The lowermost region is an infinitely extending exponentially graded heterogeneous half-space. There is sliding interface with dimensionless sliding parameter η between uppermost layer M_1 and M_2, such that

$\eta = 0$ represents welded contact,

$\eta = 1$ represents smooth contact,

$0 < \eta < 1$ represents partial sliding contact.

For the study of propagation of torsional wave, cylindrical polar coordinates (r, θ, z) system is considered. The displacement vector $\boldsymbol{u} = (0, v, 0)$ is function of r, z, t only, independent of θ. The physical configuration and boundary interfaces are depicted schematically in Fig. 1.

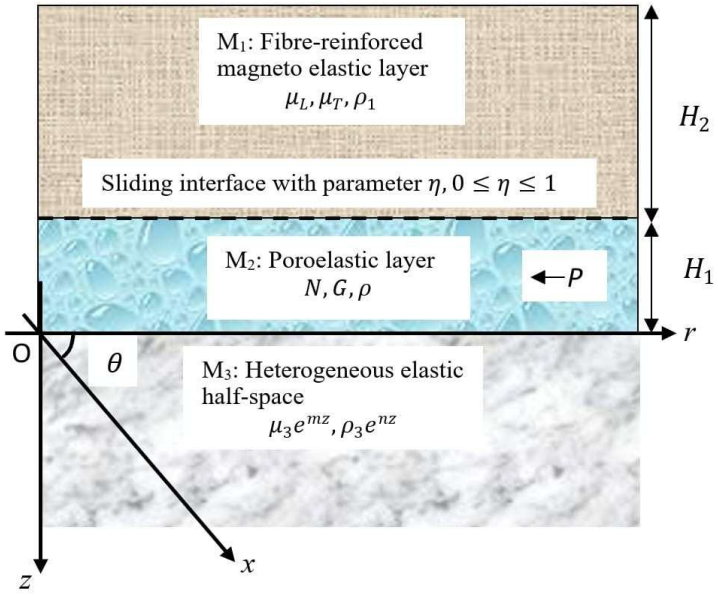


Fig. 1 Geometry of the problem

3. SOLUTIONS

3.1. SOLUTION FOR M1

Relation of stress–strain in fibre-reinforced, transversely isotropic elastic layer with preferred direction denoted by unit vector $\boldsymbol{a}$ (Belfield *et al.*) [12] is

$$\tau_{ij} = \lambda e_{kk}\delta_{ij} + 2\mu_T e_{ij} + \alpha\left(a_k a_m e_{km}\delta_{ij} + a_i a_j e_{kk}\right)$$

$$+2(\mu_L - \mu_T)\left(a_i a_k e_{kj} + a_j a_k e_{ki}\right) + \beta(a_k a_m e_{km} a_i a_j) \quad (1)$$

where λ, μ_L, μ_T, α and β are elastic constants (stress units), with μ_L and μ_T denoting longitudinal and transverse shear moduli, respectively. The electromechanical coupling in the FRME layer is governed by equations of Maxwell and Ohm

$$\nabla \times \boldsymbol{H} = \boldsymbol{J}, \nabla \times \boldsymbol{E} = -\frac{\partial \boldsymbol{B}}{\partial t}, \nabla \cdot \boldsymbol{B} = \boldsymbol{0}, \boldsymbol{B} = \mu_e \boldsymbol{H},$$

$$\left(\tau_{ij}\right)^M = \mu_e(H_i h_j + H_j h_i - H_k h_k \delta_{ij}), \quad (2)$$

$$\boldsymbol{J} = \sigma(\boldsymbol{E} + \frac{\partial \boldsymbol{u}}{\partial t} \times \boldsymbol{B})$$

$\boldsymbol{B}$ denotes magnetic induction, $\boldsymbol{E}$ electric field, $\boldsymbol{J}$ current density, μ_e is permeability of free space, σ denotes electrical conductivity of the medium, $\boldsymbol{H} = (H_r, H_\theta, H_z)$ is magnetic field, $\boldsymbol{h} = (h_r, h_\theta, h_z)$ is its perturbation.

For torsional waves propagation in fibre-reinforced medium, the equation of motion with Lorentz body force $\boldsymbol{J} \times \boldsymbol{B}$ and the associated stress components is

$$\frac{\partial \tau_{r\theta}}{\partial r} + \frac{\partial \tau_{\theta z}}{\partial z} + \frac{2\tau_{r\theta}}{r} + (\boldsymbol{J} \times \boldsymbol{B})_\theta = \rho_1 \frac{\partial^2 v}{\partial t^2}$$

$$\tau_{\theta z} = C \frac{\partial v}{\partial z} + B\left(\frac{\partial v}{\partial r} - \frac{v}{r}\right), \tau_{r\theta} = A\left(\frac{\partial v}{\partial r} - \frac{v}{r}\right) + B \frac{\partial v}{\partial z} \quad (3)$$

where ρ_1 is the material density of the layer, $A = \mu_T + (\mu_L - \mu_T)a_1^2$, $B = (\mu_L - \mu_T)a_1 a_3$, $C = \mu_T + (\mu_L - \mu_T)a_3^2$ and a_i $(i = 1, 3)$ indicates reinforcement directional unit vector components, i.e., $\boldsymbol{a} = (a_1, 0, a_3)$, so that $a_1^2 + a_3^2 = 1$.

From Eq. (2), Laplacian of $\boldsymbol{H}$ is given by

$$\nabla^2 \boldsymbol{H} = \sigma \mu_e \left[\frac{\partial \boldsymbol{H}}{\partial t} - \nabla \times \left(\frac{\partial \boldsymbol{u}}{\partial t} \times \boldsymbol{H}\right)\right] \quad (4)$$

For $\sigma \to \infty$ (perfectly conducting), Eq. (4) implies $\frac{\partial \boldsymbol{H}}{\partial t}$ and its θ-component as

$$\frac{\partial \boldsymbol{H}}{\partial t} = \nabla \times \left(\frac{\partial \boldsymbol{u}}{\partial t} \times \boldsymbol{H}\right)$$

$$\frac{\partial H_\theta}{\partial t} = \frac{\partial}{\partial r}\left(H_r \frac{\partial v}{\partial t}\right) + \frac{\partial}{\partial z}\left(H_z \frac{\partial v}{\partial t}\right) \quad (5)$$

Eqs. (4) – (5) clearly imply $\frac{\partial H_r}{\partial t} = 0$, $\frac{\partial H_z}{\partial t} = 0$ (H_r and H_z has no perturbation with time t. Only small perturbation h_θ is introduced, such that

$$H_r = H_{01}, H_\theta = H_{02} + h_\theta, H_z = H_{03}$$

with $\boldsymbol{H_0} = (H_{01}, H_{02}, H_{03}) = (H_0 \cos\varphi, 0, H_0 \sin\varphi)$, $H_0 = |\boldsymbol{H_0}|$, $\varphi =$ angle between wave vector and $\boldsymbol{H}$.

Substituting $\boldsymbol{H} = (H_0 \cos\varphi, h_\theta, H_0 \sin\varphi)$ into Eq. (5), we get

$$h_\theta = H_0\left(\frac{\partial v}{\partial r}\cos\varphi + \frac{\partial v}{\partial z}\sin\varphi\right)$$

Only non-zero Lorentz force component (in θ-direction) is

$$(\boldsymbol{J} \times \boldsymbol{B})_\theta = \mu_e H_0^2 \left(\frac{\partial^2 v}{\partial r^2}\cos^2\varphi + \frac{\partial^2 v}{\partial z^2}\sin^2\varphi + \frac{\partial^2 v}{\partial r \partial z}\sin 2\varphi\right) \quad (6)$$

From Eqs. (3) and (6), we obtain

$$P \frac{\partial^2 v}{\partial r^2} + Q \frac{\partial^2 v}{\partial z^2} + R \frac{\partial^2 v}{\partial r \partial z} + \frac{A}{r}\frac{\partial v}{\partial r} + \frac{B}{r}\frac{\partial v}{\partial z} - \frac{A}{r^2} v = \rho_1 \frac{\partial^2 v}{\partial t^2} \quad (7)$$

with $P = A + \mu_e H_0^2 \cos^2\varphi$, $Q = C + \mu_e H_0^2 \sin^2\varphi$, $R = 2B + \mu_e H_0^2 \sin 2\varphi$.

For Eq. (7), solution is considered as

$$v(r,z,t) = V(z)J_1(kr)e^{-i\omega t} \tag{8}$$

$J_1(kr)$ is Bessel's function, k is wave number, $\omega = kc$ (torsional wave speed c).

$V(z)$ satisfies

$$m_1 \frac{\partial^2 V}{\partial z^2} + m_2 \frac{\partial V}{\partial z} + m_3 V = 0 \tag{9}$$

where $m_1 = QJ_1(kr)$, $m_2 = RkJ_1'(kr) + \frac{B}{r}J_1(kr)$,

$m_3 = Pk^2 J_1''(kr) + \frac{Ak}{r}J_1'(kr) - \frac{A}{r^2}J_1(kr) + \rho_1\omega^2 J_1(kr)$.

The general solution of Eq. (9) is

$$V = (A_1 e^{\delta_1 z} + B_1 e^{-\delta_2 z}) \tag{10}$$

where $\delta_{1,2} = \frac{1}{2m_1}\left[\mp m_2 + \sqrt{m_2^2 - 4m_1 m_3}\right]$

Hence, torsional displacement for FRME layer is

$$v = (A_1 e^{\delta_1 z} + B_1 e^{-\delta_2 z})J_1(kr)e^{-i\omega t} \tag{11}$$

3.2. SOLUTION FOR M_2

Governing equations (Biot - Weiskopf) [2]-[5] are

$$\frac{\partial s_{rr}}{\partial r} + \frac{1}{r}\frac{\partial s_{r\theta}}{\partial \theta} + \frac{\partial s_{rz}}{\partial z} + \frac{s_{rr} - s_{\theta\theta}}{r} - P\left(\frac{\partial \omega_z}{\partial \theta} - \frac{\partial \omega_\theta}{\partial z}\right) = \frac{\partial^2}{\partial t^2}(\rho_{rr}u + \rho_{r\theta}U) \tag{12}$$

$$\frac{\partial s_{r\theta}}{\partial r} + \frac{1}{r}\frac{\partial s_{\theta\theta}}{\partial \theta} + \frac{\partial s_{\theta z}}{\partial z} + \frac{2}{r}s_{r\theta} - P\frac{\partial \omega_z}{\partial r} = \frac{\partial^2}{\partial t^2}(\rho_{rr}v + \rho_{r\theta}V) \tag{13}$$

$$\frac{\partial s_{rz}}{\partial r} + \frac{1}{r}\frac{\partial s_{\theta z}}{\partial \theta} + \frac{\partial s_{zz}}{\partial z} + \frac{1}{r}s_{rz} - P\frac{\partial \omega_\theta}{\partial r} = \frac{\partial^2}{\partial t^2}(\rho_{rr}w + \rho_{r\theta}W) \tag{14}$$

$$\frac{\partial s}{\partial r} = \frac{\partial^2}{\partial t^2}(\rho_{r\theta}u + \rho_{\theta\theta}U) \tag{15}$$

$$\frac{\partial s}{\partial \theta} = \frac{\partial^2}{\partial t^2}(\rho_{r\theta}v + \rho_{\theta\theta}V) \tag{16}$$

$$\frac{\partial s}{\partial z} = \frac{\partial^2}{\partial t^2}(\rho_{r\theta}w + \rho_{\theta\theta}W) \tag{17}$$

s_{ij} are incremental stress components; (u,v,w), (U,V,W) denote solid, fluid displacement components respectively, s represents fluid stress, P is initial stress. The components of the rotation vector ω are

$$\omega_r = \frac{1}{2r}\left[\frac{\partial w}{\partial \theta} - r\frac{\partial v}{\partial z}\right], \omega_\theta = \frac{1}{2}\left[\frac{\partial u}{\partial z} - \frac{\partial w}{\partial r}\right], \omega_z = \frac{1}{2r}\left[\frac{\partial (rv)}{\partial r} - \frac{\partial v}{\partial \theta}\right] \tag{18}$$

The well-known stress-strain relations given as

$$s_{rr} = (A+P)e_{rr} + (A-2N+P)e_{\theta\theta} + (F+P)e_{zz} + Q\varepsilon,$$

$$s_{\theta\theta} = (A-2N)e_{rr} + Ae_{\theta\theta} + Fe_{zz} + Q\varepsilon,$$

$$s_{zz} = Fe_{rr} + Fe_{\theta\theta} + Ce_{zz} + Q\varepsilon,$$

$$s_{r\theta} = 2Ne_{r\theta}, s_{\theta z} = 2Ge_{\theta z}, s_{rz} = 2Ge_{zr} \tag{19}$$

A, F, C, N, G are elastic constants; N, G also represent respective shear moduli of anisotropic layer in r-, z-directions, $Q > 0$ denotes coupling parameter which links volumetric strains of solid and fluid, and the strain components are

$$e_{rr} = \frac{1}{2}\frac{\partial u}{\partial r}, e_{\theta\theta} = \frac{1}{2}\left[\frac{1}{r}\frac{\partial v}{\partial \theta} + \frac{u}{r}\right], e_{zz} = \frac{1}{2}\frac{\partial w}{\partial z},$$
$$e_{r\theta} = \frac{1}{2}\left[\frac{1}{r}\frac{\partial u}{\partial \theta} + \frac{\partial v}{\partial r} - \frac{v}{r}\right], e_{\theta z} = \frac{1}{2}\left[\frac{\partial v}{\partial z} + \frac{1}{r}\frac{\partial w}{\partial \theta}\right], \tag{20}$$
$$e_{zr} = \frac{1}{2}\left[\frac{\partial w}{\partial r} + \frac{\partial u}{\partial z}\right], \varepsilon = \left[\frac{1}{r}\frac{\partial (rU)}{\partial r} + \frac{1}{r}\frac{\partial V}{\partial \theta} + \frac{\partial W}{\partial z}\right]$$

The fluid pressure p and stress s in fluid phase are related as

$$-s = fp \tag{21}$$

where f represents porosity.

The mass densities of solid phase ρ_s, fluid phase ρ_f, and porous medium ρ are connected to the mass coefficients ρ_{rr}, $\rho_{r\theta}$, $\rho_{\theta\theta}$ by the relations

$$\rho_{rr} + \rho_{r\theta} = (1-f)\rho_s,\ \rho_{r\theta} + \rho_{\theta\theta} = f\rho_f \tag{22}$$

The aggregate mass density is

$$\rho = \rho_s + f(\rho_f - \rho_s) \tag{23}$$

According to Biot's theory, the following inequalities must be satisfied to ensure physical validity

$$\rho_{r\theta} < 0, \rho_{rr} > 0,\ \rho_{\theta\theta} > 0, \rho_{rr}\rho_{\theta\theta} - \rho_{r\theta}^2 > 0 \tag{24}$$

For torsional wave motion, we assume

$$u = 0 = w, v = v(r, z, t)$$
$$U = 0 = W, V = V(r, z, t) \tag{25}$$

Under these assumptions, the only non-zero relations from Eq. (19) are

$$s_{\theta z} = 2Ge_{\theta z}, s_{r\theta} = 2Ne_{r\theta} \tag{26}$$

Substituting these expressions into Eqs. (12) - (17), the single non-zero governing equation becomes

$$\frac{\partial s_{r\theta}}{\partial r} + \frac{\partial s_{\theta z}}{\partial z} + \frac{2}{r}s_{r\theta} - P\frac{\partial \omega_z}{\partial r} = \frac{\partial^2}{\partial t^2}(\rho_{rr}v + \rho_{r\theta}V) \tag{27}$$

and $$\frac{\partial^2}{\partial t^2}(\rho_{r\theta}v + \rho_{\theta\theta}V) = 0 \tag{28}$$

By applying the stress-strain relations from Eq. (19) into Eq. (27), we obtain

$$\left(N - \frac{P}{2}\right)\left(\frac{\partial^2 v}{\partial r^2} + \frac{1}{r}\frac{\partial v}{\partial r} - \frac{v}{r^2}\right) + G\frac{\partial^2 v}{\partial z^2} = \frac{\partial^2}{\partial t^2}(\rho_{rr}v + \rho_{r\theta}V) \tag{29}$$

Using Eq. (28), we assume $\rho_{r\theta}v + \rho_{\theta\theta}V = d''$ (constant), which gives

$$V = \frac{d'' - \rho_{r\theta}v}{\rho_{\theta\theta}}$$

Therefore, $$\frac{\partial^2}{\partial t^2}(\rho_{r\theta}v + \rho_{\theta\theta}V) = d'\frac{\partial^2 v}{\partial t^2} \tag{30}$$

where $d' = \rho_{rr} - \frac{\rho_{r\theta}^2}{\rho_{\theta\theta}}$

Using this into Eq. (29), we obtain

$$\left(N - \frac{P}{2}\right)\left(\frac{\partial^2 v}{\partial r^2} + \frac{1}{r}\frac{\partial v}{\partial r} - \frac{v}{r^2}\right) + G\frac{\partial^2 v}{\partial z^2} = d'\frac{\partial^2 v}{\partial t^2} \tag{31}$$

The torsional wave speeds are $\left[\frac{N-\frac{P}{2}}{d'}\right]^{\frac{1}{2}}$ and $\left(\frac{G}{d'}\right)^{\frac{1}{2}}$ in r- and z-directions.

For porous media, the radial shear wave velocity is

$$\beta' = \left[\frac{1-\zeta}{d}c_2^2\right]^{\frac{1}{2}}$$

where $c_2 = \sqrt{\frac{N}{\rho}},\ \zeta = \frac{P}{2N},\ d = \frac{d'}{\rho} = \frac{1}{\rho}\left(\rho_{rr} - \frac{\rho_{r\theta}^2}{\rho_{\theta\theta}}\right) = \gamma_{11} - \frac{\gamma_{12}^2}{\gamma_{22}};\ \gamma_{11} = \frac{\rho_{rr}}{\rho}, \gamma_{12} = \frac{\rho_{r\theta}}{\rho}, \gamma_{22} = \frac{\rho_{\theta\theta}}{\rho}$ are Biot's non-dimensional mass parameters.

Introducing $\xi = \xi_0 + \frac{z}{L}$ and $R = \frac{r}{L}$ (non-dimensional coordinates) where $k = \frac{1}{L}$, Eq. (31) becomes

$$\frac{\partial^2 v}{\partial R^2} + \frac{1}{R}\frac{\partial v}{\partial R} - \frac{v}{R^2} + \frac{G}{N-\frac{P}{2}}\frac{\partial^2 v}{\partial \xi^2} = \frac{d'L^2}{N-\frac{P}{2}}\frac{\partial^2 v}{\partial t^2} \tag{32}$$

Assuming $v = v_1(\xi)J_1(R)e^{-i\omega t}$. $v_1(\xi)$ satisfies

$$\frac{d^2 v_1}{d\xi^2} + q^2 v_1 = 0 \tag{33}$$

where $q^2 = \frac{\left(\frac{\omega^2 L^2 d'}{N-\frac{P}{2}} - 1\right)}{\frac{G}{N-\frac{P}{2}}}$

The solution is $v_1(\xi) = A_2 e^{iq\xi} + B_2 e^{-iq\xi}$, giving the complete displacement

$$v = \left(A_2 e^{iq\xi} + B_2 e^{-iq\xi}\right)J_1(R)e^{-i\omega t} \tag{34}$$

where $q^2 = dv\left(\frac{c^2}{c_2^2} - \frac{1-\zeta}{d}\right)$, $v = \frac{N}{G}$, and $c = \omega L$ the phase velocity.

3.3. SOLUTION FOR M_3

Equation of motion is governed by

$$\frac{\partial \sigma_{r\theta}}{\partial r} + \frac{\partial \sigma_{z\theta}}{\partial z} + \frac{2}{r}\sigma_{r\theta} = \rho(z)\frac{\partial^2 v}{\partial t^2} \tag{35}$$

$v(r, \theta, z)$ being circumferential displacement, ρ as density, and $\sigma_{r\theta}$, $\sigma_{z\theta}$ as stress components. The constitutive relations are

$$\sigma_{r\theta} = \mu\left[\frac{\partial v}{\partial r} - \frac{v}{r}\right], \sigma_{z\theta} = \mu\frac{\partial v}{\partial z} \tag{36}$$

Substitution into Eq. (35) yields

$$\mu(z)\left(\frac{\partial^2 v}{\partial r^2} + \frac{1}{r}\frac{\partial v}{\partial r} - \frac{v}{r^2}\right) + \frac{\partial}{\partial z}\left\{\mu(z)\frac{\partial v}{\partial z}\right\} = \rho(z)\frac{\partial^2 v}{\partial t^2} \tag{37}$$

Assuming a separable solution

$$v = V(z)J_1(kr)e^{-i\omega t} \tag{38}$$

reduces Eq. (37) to

$$V''(z) + \frac{\mu'(z)}{\mu(z)}V'(z) - k^2\left(1 - \frac{c^2}{c_z^2}\right)V(z) = 0 \tag{39}$$

where $c_z = \sqrt{\frac{\mu}{\rho}}$.

Given the variations for rigidity and density as

$$\mu = \mu_3 e^{mz}, \rho = \rho_3 e^{nz} \tag{40}$$

Substituting these relations into the differential equation (39), we obtain

$$V''(z) + mV'(z) - k^2\left[1 - \frac{c^2 e^{nz}}{c_3^2 e^{mz}}\right]V(z) = 0 \tag{41}$$

where $c_3 = \sqrt{\frac{\mu_3}{\rho_3}}$

Eliminating $V'(z)$ from Eq. (41) by introducing $V(z) = \varphi(z)e^{\left(\frac{-mz}{2}\right)}$, we get

$$\varphi''(z) - \left[\frac{m^2}{4} + k^2\left\{1 - \frac{c^2}{c_3^2}\frac{(1+nz)}{(1+mz)}\right\}\right]\varphi(z) = 0 \tag{42}$$

Assuming the dimensionless variables $\gamma_3 = \left(1 + \frac{m^2}{4k^2} - \frac{nc^2}{mc_3^2}\right)^{\frac{1}{2}}$, $\eta_3 = \frac{2\gamma_3 k}{m}(1 + mz)$, and taking $\varphi(z) = \psi(\eta_3)$, Eq. (42) transforms into

$$\psi''(\eta_3) - \left[\frac{1}{4} - \frac{S}{\eta_3}\right]\psi(\eta_3) = 0 \tag{43}$$

where $S = \frac{c^2(m-n)k}{2c_3^2 m^2 \gamma_3}$

The displacement in half-space is required to satisfy Sommerfeld radiation condition, expressed as $\lim_{z\to\infty} v(z) = 0$. The bounded solution satisfying this condition is

$$\psi(\eta_3) = DW_{S,\frac{1}{2}}(\eta_3)$$

where $W_{S,\frac{1}{2}}(\eta_3)$ represents Whittaker function and D is arbitrary constant.

Hence, torsional displacement obtained here is

$$v = V(z)J_1(kr)e^{-i\omega t}$$

$$= \varphi(z)e^{\left(\frac{-mz}{2}\right)}J_1(kr)e^{-i\omega t}$$

$$= \left[DW_{S,\frac{1}{2}}\left(\frac{2\gamma_3 k}{m}(1 + mz)\right)\right]e^{\left(\frac{-mz}{2}\right)}J_1(kr)e^{-i\omega t} \tag{44}$$

4. BOUNDARY CONDITIONS

(i) At common interface of M_2 and M_3 ($z = 0$), both displacement and stress components must remain continuous.

(a) $[v]_2 = [v]_3$

(b) $[s_{\theta z}]_2 = [\sigma_{\theta z}]_3$

(ii) At the common sliding interface between M_1 and M_2 ($z = -H_1$) with dimensionless sliding parameter η, displacement and stress components must remain continuous.

(a) $(1-\eta)kF[v]_1 = \eta[s_{\theta z}]_2 + (1-\eta)kF[v]_2$

(b) $[\tau_{\theta z} + (\tau_{\theta z})^M]_1 = (1-\eta)[s_{\theta z}]_2$

A constant F, having the dimension of stress (force per unit area), is introduced to maintain dimensional consistency across the interface.

(iii) Stress components vanish at free surface of M_1 ($z = -(H_1 + H_2)$)

$[\tau_{\theta z} + (\tau_{\theta z})^M]_1 = 0$

5. DISPERSION RELATION

On solving boundary conditions, we obtain

$$A_2 e^{iq\xi_0} + B_2 e^{-iq\xi_0} - DK_1 = 0 \tag{45}$$

$$A_2 K_2 e^{iq\xi_0} - B_2 K_2 e^{-iq\xi_0} - DK_3 = 0 \tag{46}$$

$$A_1 K_4 e^{-\delta_1 H_1} + B_1 K_4 e^{\delta_2 H_1} - A_2 K_5 e^{iq(\xi_0 - kH_1)} + B_2 K_6 e^{-iq(\xi_0 - kH_1)} = 0 \tag{47}$$

$$A_1 K_7 e^{-\delta_1 H_1} + B_1 K_8 e^{\delta_2 H_1} - A_2 K_2 K_9 e^{iq(\xi_0 - kH_1)} + B_2 K_2 K_9 e^{-iq(\xi_0 - kH_1)} = 0 \tag{48}$$

$$A_1 K_{10} e^{-\delta_1 (H_1 + H_2)} + B_1 K_{11} e^{\delta_2 (H_1 + H_2)} = 0 \tag{49}$$

where

$K_1 = W_{S,\frac{1}{2}}\left(\frac{2\gamma_3 k}{m}\right)$, $K_2 = iGqk$,

$$K_3 = \mu_3 \left(\frac{2\gamma_3 k}{m}\right)^S e^{\frac{-\gamma_3 k}{m}} \left[\frac{-m^2}{2\gamma_3 k}\left\{\frac{1}{4} - \left(S - \frac{1}{2}\right)^2\right\} + \left(mS - \gamma_3 k - \frac{m}{2}\right)\left\{1 + \frac{m}{2\gamma_3 k}\left\{\frac{1}{4} - \left(S - \frac{1}{2}\right)^2\right\}\right\}\right],$$

$K_4 = (1-\eta)F$, $K_5 = iGq\eta + (1-\eta)F$, $K_6 = iGq\eta - (1-\eta)F$,

$$K_7 = C\delta_1 J_1(kr) + B\left[-H_1 k\delta_1' J_1(kr) + kJ_1'(kr) - \frac{J_1(kr)}{r}\right]$$

$$+\mu_e H_0^2 \sin\varphi\,[\cos\varphi\,\{-H_1 k\delta_1' J_1(kr) + kJ_1'(kr)\} + \sin\varphi\,\delta_1 J_1(kr)],$$

$$K_8 = -C\delta_2 J_1(kr) + B\left[H_1 k\delta_2' J_1(kr) + kJ_1'(kr) - \frac{J_1(kr)}{r}\right]$$

$$+\mu_e H_0^2 \sin\varphi\,[\cos\varphi\,\{H_1 k\delta_2' J_1(kr) + kJ_1'(kr)\} - \sin\varphi\,\delta_2 J_1(kr)],$$

$$K_9 = (1-\eta)J_1(kr),$$

$$K_{10} = C\delta_1 J_1(kr) + B\left[-(H_1+H_2)k\delta_1' J_1(kr) + kJ_1'(kr) - \frac{J_1(kr)}{r}\right]$$

$$+\mu_e H_0^2 \sin\varphi\,[\cos\varphi\,\{-(H_1+H_2)k\delta_1' J_1(kr) + kJ_1'(kr)\} + \sin\varphi\,\delta_1 J_1(kr)],$$

$$K_{11} = -C\delta_2 J_1(kr) + B\left[(H_1+H_2)k\delta_2' J_1(kr) + kJ_1'(kr) - \frac{J_1(kr)}{r}\right]$$

$$+\mu_e H_0^2 \sin\varphi\,[\cos\varphi\,\{(H_1+H_2)k\delta_2' J_1(kr) + kJ_1'(kr)\} - \sin\varphi\,\delta_2 J_1(kr)]$$

Eliminating A_1, B_1, A_2, B_2, D from Eqs. (45) - (49) yields

$$\begin{vmatrix} 0 & 0 & e^{iq\xi_0} & e^{-iq\xi_0} & -K_1 \\ 0 & 0 & K_2 e^{iq\xi_0} & -K_2 e^{-iq\xi_0} & -K_3 \\ K_4 e^{-\delta_1 H_1} & K_4 e^{\delta_2 H_1} & -K_5 e^{iq(\xi_0 - kH_1)} & K_6 e^{-iq(\xi_0 - kH_1)} & 0 \\ K_7 e^{-\delta_1 H_1} & K_8 e^{\delta_2 H_1} & -K_2 K_9 e^{iq(\xi_0 - kH_1)} & K_2 K_9 e^{-iq(\xi_0 - kH_1)} & 0 \\ K_{10} e^{-\delta_1(H_1+H_2)} & K_{11} e^{\delta_2(H_1+H_2)} & 0 & 0 & 0 \end{vmatrix} = 0$$

$$\Rightarrow \left(K_4 K_{10} e^{-\delta_1(H_1+H_2)+\delta_2 H_1} - K_4 K_{11} e^{-\delta_1 H_1 + \delta_2(H_1+H_2)}\right)\left[-K_1 K_2^2 K_9\left(e^{iqkH_1} - e^{-iqkH_1}\right)\right.$$
$$\left. + K_2 K_3 K_9\left(e^{iqkH_1} + e^{-iqkH_1}\right)\right]$$

$$-\left(K_8 K_{10} e^{-\delta_1(H_1+H_2)+\delta_2 H_1} - K_7 K_{11} e^{-\delta_1 H_1 + \delta_2(H_1+H_2)}\right)\left[-K_1 K_2\left(K_6 e^{iqkH_1} - K_5 e^{-iqkH_1}\right) + \right.$$
$$\left. K_3\left(K_6 e^{iqkH_1} + K_5 e^{-iqkH_1}\right)\right] = 0 \qquad (50)$$

which gives the dispersion relation for torsional wave.

5.1. VALIDATION OF THE PROBLEM

When the medium is assumed with no magnetic field, no fibres, no sliding interface, non-porous, stress-free, homogeneous, and then the upper layer is neglected, the system reduces to

isotropic elastic layer on top of isotropic elastic half-space. We make following assumptions for this:

For upper layer M_1: Assume $H_0 = 0$ (removing static magnetic field), $\mu_L \to \mu_T \to \mu_1$ (say, neglecting anisotropy due to fibres), $H_2 = 0$ (neglecting upper layer M_1).

For sliding interface: $\eta = 0$ (making welded contact)

For middle layer M_2: Assume $N \to G \to \mu_2$ (say, making directional rigidities equal), $P = 0$ (neglecting initial stress) $\Rightarrow \zeta = 0$, $f = 0$ (making medium non-porous solid)

For lower half-space M_3: Assume $m \to n \to 0$ (neglecting heterogeneity)

In these limiting conditions, (Eq. 50) gets reduced to Love wave equation

$$tan\left(kH_1\sqrt{\frac{c^2}{c_2^2}-1}\right) = \frac{\mu_3}{\mu_2}\frac{\sqrt{1-\frac{c^2}{c_3^2}}}{\sqrt{\frac{c^2}{c_2^2}-1}}$$

5.2. PARTICULAR CASES

5.2.1. Case I: On making welded contact, i.e. $\eta = 0$, as a result Eq. (50) becomes

$$\left(FK_{10}e^{-\delta_1(H_1+H_2)+\delta_2H_1} - FK_{11}e^{-\delta_1H_1+\delta_2(H_1+H_2)}\right)\left[-K_1K_2^2J_1(kr)\left(e^{iqkH_1} - e^{-iqkH_1}\right)\right.$$
$$\left. + K_2K_3J_1(kr)\left(e^{iqkH_1} + e^{-iqkH_1}\right)\right]$$

$$-\left(K_8K_{10}e^{-\delta_1(H_1+H_2)+\delta_2H_1} - K_7K_{11}e^{-\delta_1H_1+\delta_2(H_1+H_2)}\right)\left[-K_1K_2\left(-Fe^{iqkH_1} - Fe^{-iqkH_1}\right)\right.$$
$$\left. + K_3\left(-Fe^{iqkH_1} + Fe^{-iqkH_1}\right)\right] = 0$$

5.2.2. Case II: On making smooth contact, i.e. $\eta = 1$, as a result Eq. (50) becomes

$$\left(FK_{10}e^{-\delta_1(H_1+H_2)+\delta_2H_1} - FK_{11}e^{-\delta_1H_1+\delta_2(H_1+H_2)}\right)$$

$$-\left(K_8K_{10}e^{-\delta_1(H_1+H_2)+\delta_2H_1} - K_7K_{11}e^{-\delta_1H_1+\delta_2(H_1+H_2)}\right)\left[-K_1K_2iGq\left(e^{iqkH_1} - e^{-iqkH_1}\right)\right.$$
$$\left. + K_3iGq\left(e^{iqkH_1} + e^{-iqkH_1}\right)\right] = 0$$

5.2.3. Case III: On neglecting pre-stress ($P = 0 \Rightarrow \zeta = 0$), neglecting porosity ($f = 0 \Rightarrow d = 1$), neglecting directional rigidities, i.e. $N \to G \to \mu_2$ (say), as a result Eq. (50) becomes

$$\left(K_4K_{10}e^{-\delta_1(H_1+H_2)+\delta_2H_1}\right.$$

$$\left.-K_4K_{11}e^{-\delta_1H_1+\delta_2(H_1+H_2)}\right)\left[K_1\left(\mu_2k\sqrt{\frac{c^2}{c_2^2}-1}\right)^2K_9\left(e^{ikH_1\sqrt{\frac{c^2}{c_2^2}-1}}\right.\right.$$

$$\left.\left.-e^{-ikH_1\sqrt{\frac{c^2}{c_2^2}-1}}\right)+i\mu_2k\sqrt{\frac{c^2}{c_2^2}-1}K_3K_9\left(e^{ikH_1\sqrt{\frac{c^2}{c_2^2}-1}}+e^{-ikH_1\sqrt{\frac{c^2}{c_2^2}-1}}\right)\right]$$

$$-\left(K_8K_{10}e^{-\delta_1(H_1+H_2)+\delta_2H_1}\right.$$

$$\left.-K_7K_{11}e^{-\delta_1H_1+\delta_2(H_1+H_2)}\right)\left[-K_1i\mu_2k\sqrt{\frac{c^2}{c_2^2}-1}\left\{\left(i\eta\mu_2\sqrt{\frac{c^2}{c_2^2}-1}\right.\right.\right.$$

$$\left.\left.-(1-\eta)F\right)e^{ikH_1\sqrt{\frac{c^2}{c_2^2}-1}}-\left(i\eta\mu_2\sqrt{\frac{c^2}{c_2^2}-1}+(1-\eta)F\right)e^{-ikH_1\sqrt{\frac{c^2}{c_2^2}-1}}\right\}$$

$$+K_3\left\{\left(i\eta\mu_2\sqrt{\frac{c^2}{c_2^2}-1}-(1-\eta)F\right)e^{ikH_1\sqrt{\frac{c^2}{c_2^2}-1}}\right.$$

$$\left.\left.+\left(i\eta\mu_2\sqrt{\frac{c^2}{c_2^2}-1}+(1-\eta)F\right)e^{-ikH_1\sqrt{\frac{c^2}{c_2^2}-1}}\right\}\right]=0$$

5.2.4. Case IV: On neglecting heterogeneities in semi-infinite space M_3, i.e. $m \to n \to 0$, as a result Eq. (50) becomes

$$\left(K_4K_{10}e^{-\delta_1(H_1+H_2)+\delta_2H_1}-K_4K_{11}e^{-\delta_1H_1+\delta_2(H_1+H_2)}\right)\left[-K_2^2K_9\left(e^{iqkH_1}-e^{-iqkH_1}\right)\right.$$

$$\left.-K_2K_9\mu_3k\sqrt{1-\frac{c^2}{c_3^2}}\left(e^{iqkH_1}+e^{-iqkH_1}\right)\right]$$

$$-\left(K_8K_{10}e^{-\delta_1(H_1+H_2)+\delta_2H_1}-K_7K_{11}e^{-\delta_1H_1+\delta_2(H_1+H_2)}\right)\Bigg[-K_2\left(K_6e^{iqkH_1}-K_5e^{-iqkH_1}\right)$$

$$-\mu_3k\sqrt{1-\frac{c^2}{c_3^2}}\left(K_6e^{iqkH_1}+K_5e^{-iqkH_1}\right)\Bigg]=0$$

6. NUMERICAL COMPUTATIONS AND DISCUSSIONS

Dispersion relation establishes functional dependence between normalized phase velocity $\frac{c}{c_2}$ and dimensionless wavenumber kH_2 which is governed by several physical parameters, including material properties of constituent media, geometrical characteristics of layered structure, initial stresses etc.

Material parameters for the three regions are selected as follows:

For M_1 [24], $\mu_L = 5.66 \times 10^9\ N/m^2$, $\mu_T = 2.46 \times 10^9\ N/m^2$, $\rho_1 = 2260\ kg/m^3$

For M_2 [25], $G = 0.1387 \times 10^{10}\ N/m^2$, $N = 0.2774 \times 10^{10}\ N/m^2$, $\rho_{rr} = 1.926137 \times 10^3\ kg/m^3$, $\rho_{r\theta} = -0.002137 \times 10^3\ kg/m^3$, $\rho_{\theta\theta} = 0.2153337 \times 10^3\ kg/m^3$

For M_3, $\mu_3 = 7.34\ \times 10^{10}\ N/m^2$, $\rho_3 = 3195\ kg/m^3$

To investigate influence of various parameters on wave propagation, dispersion equation (Eq. 50) is solved numerically for different sets of parameters. The computational and graphical analysis is carried out using *Mathematica*. In each figure, multiple curves are presented by varying a single parameter while keeping the remaining parameters fixed, allowing a clear assessment of its individual effect on wave propagation characteristics. The results consistently demonstrate that the phase velocity decreases monotonically with increasing wavenumber. This behavior confirms the dispersive nature of the medium, wherein waves of higher frequency (or shorter wavelength) propagate with lower phase velocity.

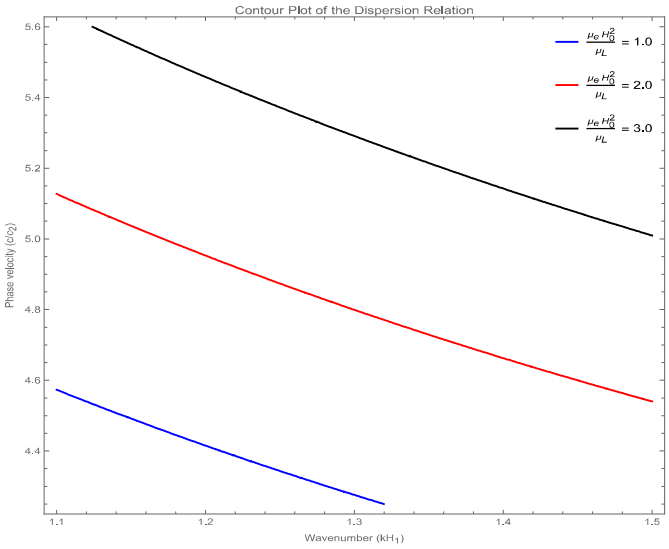


Fig. 2 Impact of magneto-elastic coupling parameter $\frac{\mu_e H_0^2}{\mu_L}$

Fig. 2 illustrates influence of coupled magneto-elastic parameter $\frac{\mu_e H_0^2}{\mu_L}$ in upper fibre-reinforced magneto-elastic layer. The parameter is assigned the values $\frac{\mu_e H_0^2}{\mu_L} = 1.0,2.0,3.0$, while the remaining parameters are fixed at $\frac{H_2}{H_1} = 1.0, kr = 3.8, (a_1^2, a_3^2) = (0.5,0.5), \varphi = \frac{\pi}{36}, \eta = 0.5, \frac{F}{G} = 1.0, \zeta = 0.1, d = 0.9, \frac{m}{k} = 1.0, \frac{n}{k} = 2.0$. The dispersion curves exhibit an upward shift with increasing values of $\frac{\mu_e H_0^2}{\mu_L}$, indicating an enhancement in phase velocity due to stronger magneto-elastic coupling.

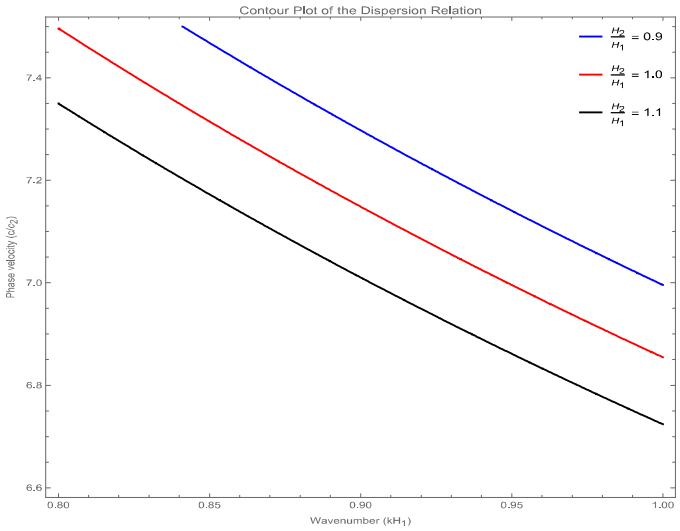


Fig. 3 Impact of depth ratio $\frac{H_2}{H_1}$

Fig. 3 presents effect of depth ratio $\frac{H_2}{H_1}$ of finite layers. The values considered are $\frac{H_2}{H_1} = 0.9,1.0,1.1$, while all other parameters remain unchanged at $\frac{\mu_e H_0^2}{\mu_L} = 5.0, kr = 3.8, (a_1^2, a_3^2) = (0.5,0.5), \varphi = \frac{\pi}{36}, \eta = 0.5, \frac{F}{G} = 1.0, \zeta = 0.1, d = 0.9, \frac{m}{k} = 1.0, \frac{n}{k} = 2.0$. The results show a downward shift in the dispersion curves as $\frac{H_2}{H_1}$ increases, suggesting a reduction in phase velocity with increasing depth of intermediate layer, and / or decreasing depth of upper layer.

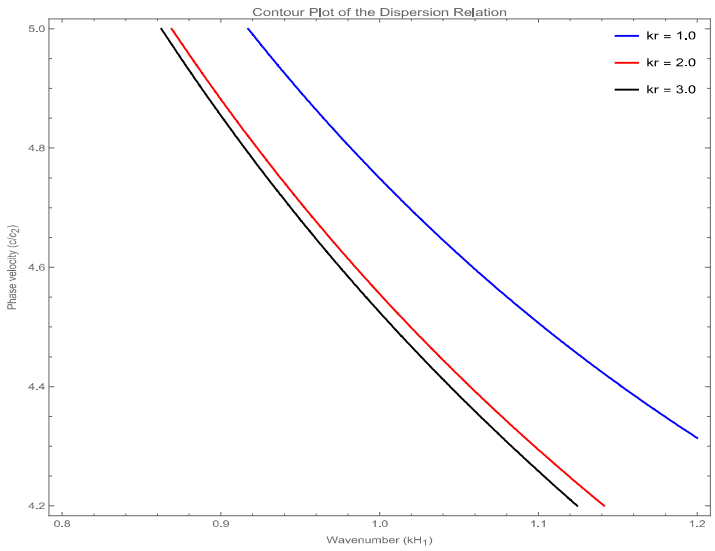


Fig. 4 Impact of dimensionless radial displacement kr

Fig. 4 depicts effect of dimensionless radial displacement kr in upper fibre-reinforced magneto-elastic layer. The parameter is varied as $kr = 1.0,2.0,3.0$, with the remaining parameters fixed at $\frac{H_2}{H_1} = 1.0, \frac{\mu_e H_0^2}{\mu_L} = 5.0, (a_1^2, a_3^2) = (0.5,0.5), \varphi = \frac{\pi}{36}, \eta = 0.5, \frac{F}{G} = 1.0, \zeta = 0.1, d = 0.9, \frac{m}{k} = 1.0, \frac{n}{k} = 2.0$. Here, dispersion curves gets lowered on increasing kr, indicating a decrease in phase velocity.

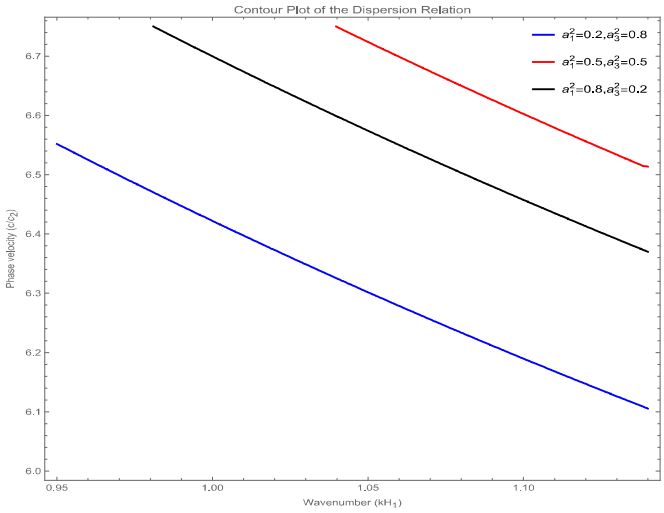


Fig. 5 Impact of variations in components of directional unit vector of reinforcement (a_1^2, a_3^2)

Fig. 5 examines effect of variations in components of directional unit vector of reinforcement (a_1^2, a_3^2) in upper layer. The parameter combinations considered are $(a_1^2, a_3^2) = (0.2,0.8), (0.5,0.5), (0.8,0.2)$, while the remaining parameters are kept fixed at $\frac{H_2}{H_1} = 1.0, \frac{\mu_e H_0^2}{\mu_L} = 5.0, kr = 3.8, \varphi = \frac{\pi}{36}, \eta = 0.5, \frac{F}{G} = 1.0, \zeta = 0.1, d = 0.9, \frac{m}{k} = 1.0, \frac{n}{k} = 2.0.$ The curve associated with higher a_1^2 (i.e., reinforcement aligned more along the direction of wave propagation) consistently shows higher phase velocity when compared with the case of larger a_3^2 (reinforcement oriented normal to the propagation direction). This behavior can be attributed to the enhanced effective rigidity of the medium along the direction of propagation when fibres are aligned with the wave path. Consequently, the resistance to deformation increases, allowing waves to propagate with greater speed.

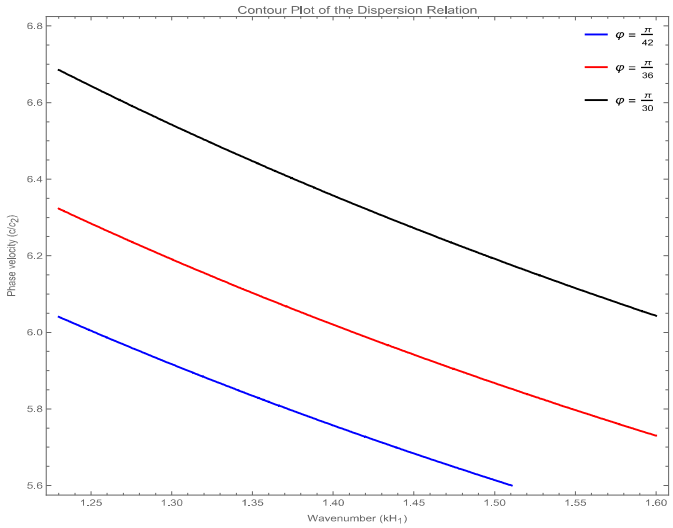


Fig. 6 Impact of angle between wave and magnetic field φ

Fig. 6 illustrates effect of angle φ between direction of wave propagation and magnetic field in upper layer. The parameter is varied as $\varphi = \frac{\pi}{42}, \frac{\pi}{36}, \frac{\pi}{30}$, while the remaining parameters are held fixed at $\frac{H_2}{H_1} = 1.0, \frac{\mu_e H_0^2}{\mu_L} = 5.0, kr = 3.8, (a_1^2, a_3^2) = (0.5,0.5), \eta = 0.5, \frac{F}{G} = 1.0, \zeta = 0.1, d = 0.9, \frac{m}{k} = 1.0, \frac{n}{k} = 2.0$. The dispersion curves exhibit an upward shift with increasing φ, indicating that phase velocity increases as angle between magnetic field and wave propagation direction becomes larger.

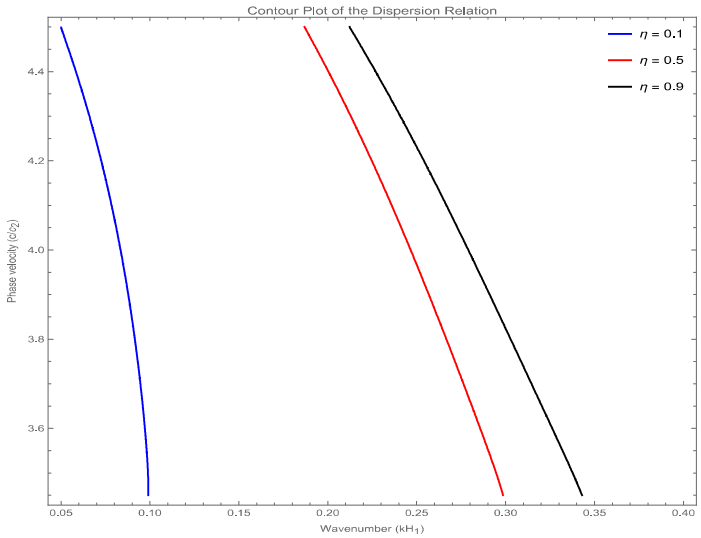


Fig. 7 Impact of sliding parameter η

Fig. 7 presents influence of sliding parameter η at interface of upper and middle layers. The values considered are $\eta = 0.1,0.5,0.9$, with all other parameters fixed at $\frac{H_2}{H_1} = 1.0, \frac{\mu_e H_0^2}{\mu_L} = 5.0, kr = 3.8, (a_1^2, a_3^2) = (0.5,0.5), \varphi = \frac{\pi}{36}, \frac{F}{G} = 1.0, \zeta = 0.1, d = 0.9, \frac{m}{k} = 1.0, \frac{n}{k} = 2.0$. The results reveal an upward shift in the dispersion curves with increasing η, suggesting that increased interfacial slip enhances phase velocity.

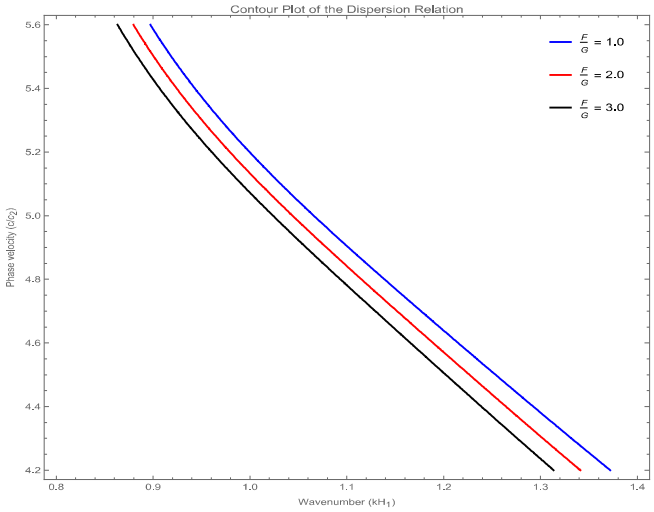


Fig. 8 Impact of dimensionless force constant $\frac{F}{G}$

Fig. 8 depicts the effect of the dimensionless force constant ratio $\frac{F}{G}$. The parameter is assigned the values $\frac{F}{G} = 1.0,2.0,3.0$, while keeping the remaining parameters fixed at $\frac{H_2}{H_1} = 1.0, \frac{\mu_e H_0^2}{\mu_L} = 5.0, kr = 3.8, (a_1^2, a_3^2) = (0.5,0.5), \varphi = \frac{\pi}{36}, \eta = 0.5, \zeta = 0.1, d = 0.9, \frac{m}{k} = 1.0, \frac{n}{k} = 2.0$. It is observed that the dispersion curves shift downward as $\frac{F}{G}$ increases, indicating a decrease in phase velocity with increasing force constant ratio.

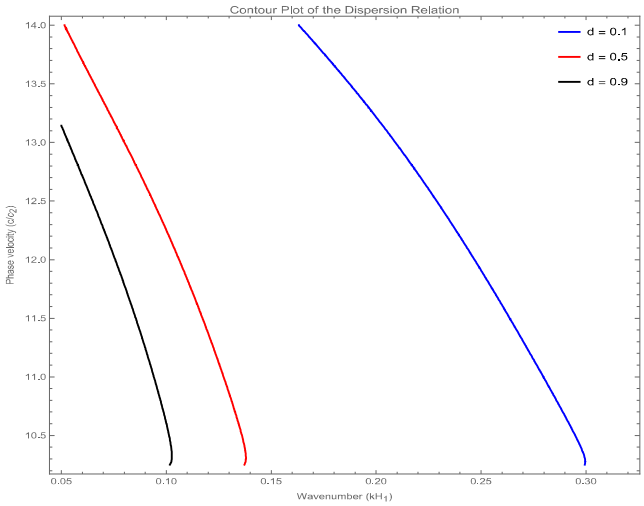


Fig. 9 Impact of the porosity parameter d

Fig. 9 examines influence of porosity parameter d in middle poroelastic layer. The parameter values considered are $d = 0.1,0.5,0.9$ with the remaining parameters fixed at $\frac{H_2}{H_1} = 1.0, \frac{\mu_e H_0^2}{\mu_L} = 5.0, kr = 3.8, (a_1^2, a_3^2) = (0.5,0.5), \varphi = \frac{\pi}{36}, \eta = 0.5, \zeta = 0.1, \frac{F}{G} = 1.0, \frac{m}{k} = 1.0, \frac{n}{k} = 2.0.$ The results indicate a downward shift in the dispersion curves with increasing d.

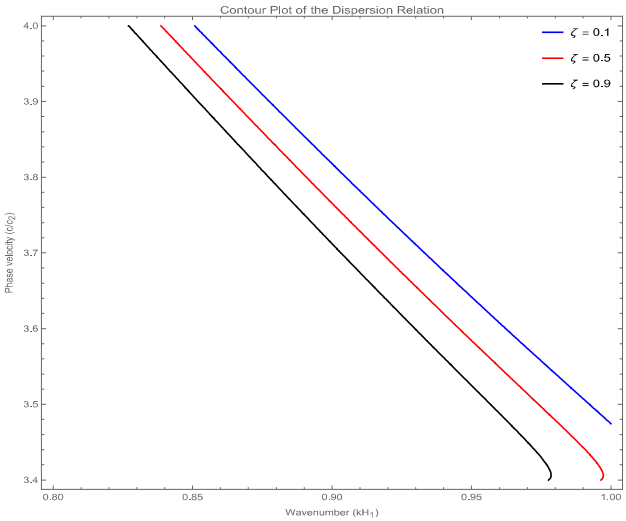


Fig. 10 Impact of dimensionless pre-stress parameter ζ

Fig. 10 illustrates effect of dimensionless pre-stress parameter ζ in intermediate poroelastic layer, which varies as $\zeta = 0.1,0.5,0.9$, while the other parameters are maintained at $\frac{H_2}{H_1} = 1.0, \frac{\mu_e H_0^2}{\mu_L} = 5.0, kr = 3.8, (a_1^2, a_3^2) = (0.5,0.5), \varphi = \frac{\pi}{36}, \eta = 0.5, d = 0.9, \frac{F}{G} = 1.0, \frac{m}{k} = 1.0, \frac{n}{k} = 2.0.$ The

dispersion curves shift downward with increasing ζ, indicating that higher initial stress reduces the phase velocity.

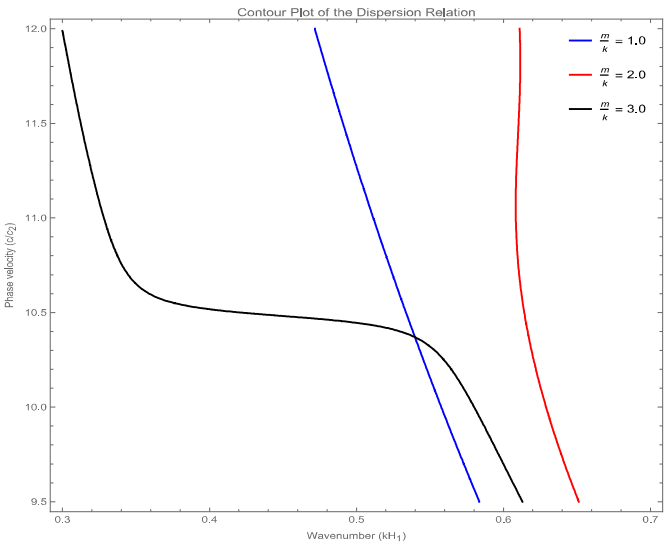


Fig. 11 Impact of dimensionless rigidity heterogeneity parameter $\frac{m}{k}$

Fig. 11 explores impact of dimensionless rigidity heterogeneity parameter $\frac{m}{k}$ in heterogeneous lower half-space. The parameter takes values $\frac{m}{k} = 1.0,2.0,3.0$ with the remaining parameters fixed as $\frac{H_2}{H_1} = 1.0, \frac{\mu_e H_0^2}{\mu_L} = 5.0, kr = 3.8, (a_1^2, a_3^2) = (0.5,0.5), \varphi = \frac{\pi}{36}, \eta = 0.5, d = 0.9, \frac{F}{G} = 1.0, \zeta = 0.1, \frac{n}{k} = 2.0$. A careful examination of the graphical trends reveals that increase in $\frac{m}{k}$ ratio makes discernible upward shift in phase velocity curves across the entire wave number spectrum. This behaviour can be attributed to the progressive stiffening of half-space as the heterogeneity parameter increases. Higher $\frac{m}{k}$ signifies more rapid increase in rigidity with depth, effectively creating a more competent substratum that offers greater resistance to shear deformation. The upward trend indicates that the half-space's heterogeneity acts as a reinforcing mechanism, pulling the dispersion curves to higher velocities. This observation is physically consistent: as the underlying medium becomes harder, the overall effective stiffness of the waveguide increases, thereby accelerating the wave.

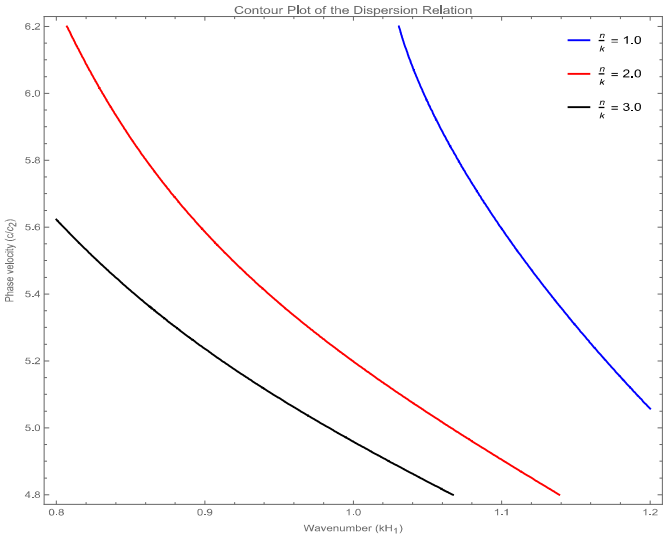


Fig. 12 Impact of dimensionless density heterogeneity parameter $\frac{n}{k}$

Fig. 12 illustrates influence of dimensionless density heterogeneity parameter $\frac{n}{k}$ in lower half-space. The parameter is varied as $\frac{n}{k} = 1.0,2.0,3.0$, while the remaining parameters are fixed at $\frac{H_2}{H_1} = 1.0, \frac{\mu_e H_0^2}{\mu_L} = 5.0, kr = 3.8, (a_1^2, a_3^2) = (0.5,0.5), \varphi = \frac{\pi}{36}, \eta = 0.5, d = 0.9, \frac{F}{G} = 1.0, \zeta = 0.1, \frac{m}{k} = 1.0$. The dispersion curves exhibit a downward shift with increasing values of $\frac{n}{k}$, indicating a reduction in phase velocity. This behavior suggests that an increase in density heterogeneity within lower semi-infinite space effectively enhances inertia medium, thereby impeding propagation of wave and resulting in lower phase velocities.

7. CONCLUSIONS

The present investigation delves into the intricate dynamics of torsional surface wave propagation within a multilayered geological structure, encompassing a fibre-reinforced magnetoelastic layer, a pre-stressed anisotropic poroelastic layer, and an exponentially graded heterogeneous half-space. Further, it uniquely incorporates a sliding interface between the upper two layers, characterized by a dimensionless parameter, thereby capturing a spectrum of bonding conditions from perfectly welded to perfectly smooth contacts.

1. Through rigorous mathematical formulation and analytical solution of the governing equations under appropriate boundary conditions, a generalised dispersion relation has been derived. This relation elegantly encapsulates the coupled influences of fibre-

reinforcement, magnetoelastic coupling, initial stress, porosity, and depth-wise heterogeneity on phase velocity.

2. Validation of formulation is firmly established by demonstrating its scaling down to classical Love wave equation as per specific simplifying assumptions, thereby harmonising with foundational knowledge in geodynamics. Subsequent numerical computations and graphical illustrations have yielded profound insights into the parametric sensitivity of characteristics of wave propagation.
3. It is observed that magnetoelastic coupling parameter and angle of magnetic field exert a reinforcing influence, elevating the phase velocity, thereby indicating that electromagnetic fields can significantly enhance the stiffness characteristics of the medium.
4. Conversely, parameters such as the depth ratio of the layers, dimensionless radial displacement, porosity parameter, initial stress, and density heterogeneity parameter of half-space consistently diminish phase velocity, reflecting their role in altering the effective impedance and energy dissipation mechanisms within the structure.
5. The sliding parameter at the interface emerges as a critical factor, with increased sliding promoting higher phase velocities, suggesting that interfacial compliance can facilitate faster wave transmission under certain conditions.

In essence, this work provides a comprehensive theoretical framework that advances the fundamental knowledge on torsional waves in complex, multi-physical media. The results may also serve as a valuable tool in seismic characterization and non-destructive evaluation of layered geological formations and engineered composites. The findings underscore the necessity of considering coupled field effects and interfacial conditions when interpreting surface wave data from real-world, heterogeneous Earth structures.

8. REFERENCES

[1] A. E. H. Love, A Treatise on the Mathematical Theory of Elasticity. Cambridge, U.K.: Cambridge Univ. Press, 1920.

[2] M. A. Biot, “Influence of initial stress on elastic waves,” J. Appl. Phys., vol. 11, no. 8, pp. 522–530, 1940, doi: 10.1063/1.1712807.

[3] W. H. Weiskopf, “Stresses in soils under a foundation,” J. Franklin Inst., vol. 239, no. 6, pp. 445–465, 1945, doi: 10.1016/0016-0032(45)90189-X.

[4] M. A. Biot, “Theory of propagation of elastic waves in a fluid-saturated porous solid. I. Low frequency range,” J. Acoust. Soc. Am., vol. 28, no. 2, pp. 168–178, 1956, doi: 10.1121/1.1908239.

[5] M. A. Biot, “Theory of propagation of elastic waves in a fluid-saturated porous solid. II. Higher frequency range,” J. Acoust. Soc. Am., vol. 28, no. 2, pp. 179–191, 1956, doi: 10.1121/1.1908241.

[6] W. M. Ewing, W. S. Jardetzky, and F. Press, Elastic Waves in Layered Media. New York, NY, USA: McGraw-Hill, 1957.

[7] M. A. Biot, Mechanics of Incremental Deformation. New York, NY, USA: John Wiley & Sons, 1965.

[8] M. Bath, Mathematical Aspects of Seismology. New York, NY, USA: Elsevier, 1968.

[9] A. Chakrabarti, “Torsional wave propagation in magneto-elastic solids with modified Maxwell stress,” ZAMM–J. Appl. Math. Mech., vol. 49, no. 12, pp. 717–727, 1969, doi: 10.1002/zamm.19690491204.

[10] D. S. Chandrasekharaiah, “On the propagation of torsional waves in magneto-viscoelastic solids,” Tensor NS, vol. 23, pp. 17–20, 1972.

[11] J. D. Achenbach, Wave Propagation in Elastic Solids. New York, NY, USA: North-Holland, 1973.

[12] A. J. Belfield, T. G. Rogers, and A. J. M. Spencer, “Stress in elastic plates reinforced by fibres lying in concentric circles,” *J. Mech. Phys. Solids*, vol. 31, no. 1, pp. 25–54, 1983, doi: 10.1016/0022-5096(83)90018-2

[13] S. Gupta, A. Chattopadhyay, and D. K. Majhi, “Effect of irregularity on the propagation of torsional surface waves in an initially stressed anisotropic poro-elastic layer,” Appl. Math. Mech. (Engl. Ed.), vol. 31, pp. 481–492, 2010, doi: 10.1007/s10483-010-0408-9.

[14] A. Chattopadhyay, S. Gupta, P. Kumari, and V. K. Sharma, “Propagation of torsional waves in an inhomogeneous layer over an inhomogeneous half-space,” Meccanica, vol. 46, pp. 671–680, 2011, doi: 10.1007/s11012-010-9329-5.

[15] S. Gupta, A. Chattopadhyay, and D. K. Majhi, “Effect of rigid boundary on propagation of torsional surface waves in porous elastic layer,” Appl. Math. Mech. (Engl. Ed.), 2011, doi: 10.1007/s10483-011-1418-6.

[16] S. Gupta, D. Majhi, S. Vishwakarma, and S. Kundu, “Propagation of torsional surface waves under the effect of irregularity and initial stress,” Appl. Math., vol. 2, pp. 1453–1461, 2011, doi: 10.4236/am.2011.212207.

[17] S. Gupta, D. K. Majhi, S. Kundu, and S. K. Vishwakarma, “Propagation of torsional surface waves in a homogeneous layer of finite thickness over an initially stressed heterogeneous half-space,” Appl. Math. Comput., vol. 218, no. 9, pp. 5655–5664, Jan. 2012, doi: 10.1016/j.amc.2011.11.060.

[18] R. Kakar and S. Kakar, “Torsional waves in prestressed fibre reinforced medium subjected to magnetic field,” J. Solid Mech., vol. 4, pp. 402–415, 2012.

[19] S. Gupta, D. K. Majhi, and S. K. Vishwakarma, “Torsional surface wave propagation in an initially stressed non-homogeneous layer over a non-homogeneous half-space,” Appl. Math. Comput., vol. 219, no. 6, pp. 3209–3218, Nov. 2012, doi: 10.1016/j.amc.2012.09.058.

[20] P. Kumari and V. K. Sharma, “Propagation of torsional waves in a viscoelastic layer over an inhomogeneous half space,” Acta Mech., vol. 225, pp. 1673–1684, 2014, doi: 10.1007/s00707-013-1021-0.

[21] P. Kumari, C. Modi, and V. K. Sharma, “Torsional waves in a magneto-viscoelastic layer over an inhomogeneous substratum,” Eur. Phys. J. Plus, vol. 131, pp. 1–11, 2016, doi: 10.1140/epjp/i2016-16263-7.

[22] A. K. Singh, A. Lakshman, and A. Chattopadhyay, “Influence of corrugated boundary surface and reinforcement of fibre-reinforced layer on propagation of torsional surface wave,” J. Vib. Control, vol. 23, pp. 1417–1436, 2017, doi: 10.1177/1077546315593838.

[23] S. K. Tomar and N. Kaur, “Role of sliding contact interface on torsional waves,” Math. Student, vol. 88, pp. 125–138, 2019.

[24] P. Kumari, S. K. Tomar, and V. K. Sharma, “Dynamical behaviour of torsional waves in a layered composite structure with sliding contact,” Arab. J. Geosci., vol. 15, p. 546, 2022, doi: 10.1007/s12517-022-09708-w.

[25] Pramanik, D., Manna, S. “Dynamic behavior of material strength due to the effect of prestress, aeolotropy, non-homogeneity, irregularity, and porosity on the propagation of torsional waves.” *Acta Mech* **233**, 1125–1146 (2022). https://doi.org/10.1007/s00707-022-03164-z

[26] Majhi, D. K., Kumar, M., Rajak, B. P., & Kundu, S. (2024). Effect of non-homogeneity and initial stress on torsional surface wave propagation in initially stressed poroelastic medium bounded by a heterogeneous layer and half-space. *Mechanics of Solids*, *59*(2), 831-845.

[27] Majhi, D.K., Kumar, M., Rajak, B.P. *et al.* Effect of initial stress and inhomogeneity on the Love wave propagation in an inhomogeneous composite structure. *Acta Mech* **236**, 3281–3294 (2025). https://doi.org/10.1007/s00707-025-04324-7

Acknowledgements The authors convey their sincere thanks to Patna University for providing facilities.

Funding This research did not receive any specific grant from funding agencies in the public, commercial, or not-for-profit sectors.

Data Availability All data that supports the finding of this study are present in the submitted article. With the help of the data and *Mathematica* software, codes were generated to plot the graphs.

Conflict of Interest The authors declared no potential conflicts of interest with respect to the research, authorship, and publication of this article.